Check for updates

Synthesis of germanium nanocrystals from solid-state disproportionation of a chloride-derived germania glass†

Yujie Wang, [ID] [a] Utkarsh Ramesh, [a] Charles K. A. Nyamekye, [bc] Bradley J. Ryan, [a]
Rainie D. Nelson, [ID] [a] Abdulla M. Alebri, [a] Umar H. Hamdeh, [a] Atefe Hadi, [a]
Emily A. Smith [ID] [bc] and Matthew G. Panthani [ID] *[a]

Germanium nanocrystals (Ge NCs) have potential to be used in several optoelectronic applications such as photodetectors and light-emitting diodes. Here, we report a solid-state route to synthesizing Ge NCs through thermal disproportionation of a germania (GeO$_X$) glass, which was synthesized by hydrolyzing a GeCl$_2$·dioxane complex. The GeO$_X$ glass synthesized in this manner was found to have residual Cl content. The process of nanocrystal nucleation and growth was monitored using powder X-ray diffraction, transmission electron microscopy, X-ray photoelectron spectroscopy and Raman spectroscopy. Compared to existing solid-state routes for synthesizing colloidal Ge NCs, this approach requires fewer steps and is amenable to scaling to large-scale reactions.

Quantum dots have tremendous potential for several opto-electronic applications due to their unique properties;[1–3] however, many quantum dot materials contain toxic elements such as Cd and Pb. This has motivated a search for other nanocrystal systems, including Group IV semiconductors (Si, Ge, and Sn).[4–6] Ge NCs are thought to be promising for a variety of applications such as light-emitting diodes,[7,8] nonvolatile memory,[9] field-effect transistors,[10] lithium ion batteries,[11] and near-infrared photodetectors.[12]

Several synthetic methods for preparing Ge NCs have been reported, including solution-phase synthesis from Zintl salts,[13,14] plasma-based synthesis,[15] thermal processing of sol–gel derived from organogermanium,[16–18] decomposition of organogermanes in supercritical fluids,[19] microwave-assisted colloidal synthesis,[20,21] and hot-injection based arrested precipitation.[7,22] Very recently, there have been reports of solid state approaches using a Ge(OH)$_2$ precursor.[23–25] These approaches used Ge(OH)$_2$ that was derived from GeO$_2$, followed by thermal annealing to induce dehydration

and disproportionation, ultimately resulting in Ge NCs suspended within a germania matrix.

In this report, we departed from this strategy by synthesizing GeO$_X$ through the hydrolysis and subsequent dehydration of GeCl$_2$.[26] Compared to previous approaches, the GeCl$_2$ precursor has the advantage of being hydrolyzed by water at room temperature to instantly form Ge(OH)$_2$, which can subsequently be dehydrated to form GeO$_X$. The GeO$_X$ was subsequently used as a solid-state precursor for synthesizing Ge NCs by thermal disproportionation. Freestanding Ge NCs could be liberated by mixing the oxide-embedded Ge NCs with deionized water to selectively etch the matrix. Further surface modification could be achieved by first hydrogen terminating the Ge NC surfaces using a hydrofluoric acid (HF) solution followed by heating in the presence of a terminal alkene to induce hydrogermylation, which resulted in alkyl-terminated Ge NCs. In a typical reaction, GeCl$_2$·dioxane was hydrolyzed with water and dried under vacuum and heated to form a yellow powder that was subsequently annealed in N$_2$ at elevated temperatures.

We use powder X-ray diffraction (XRD) to identify the processing temperature at which crystalline Ge begins to appear (Fig. 1). The XRD pattern of the hydrolyzed GeCl$_2$·dioxane (prior to annealing) exhibits broad amorphous features centered around 31.4° and 50.8° 2θ. Previous studies from Javadi *et al.*[24,25] and Sun *et al.*[23] also reported amorphous features from GeO$_2$-derived GeO prior to annealing; however these amorphous scattering features were at slightly lower angles (27.5° and 50° 2θ) and were attributed to amorphous germanium.[24,25] The different positions of the amorphous features in the precursors indicate that our samples may possess a different composition from the previous studies. Differential scanning calorimetry (DSC) reveals an exotherm that we hypothesized to coincide with the decomposition of the precursor and formation of Ge nuclei around 250 °C (Fig. S1, ESI†). From XRD pattern, the precursor remains amorphous through dehydration at 250 °C, and upon continued heating up to 325 °C. Upon heating to 325 °C, peaks corresponding to diamond cubic Ge and hexagonal GeO$_2$ emerge. At higher temperatures, the relative intensities of cubic Ge reflections

[a] Department of Chemical and Biological Engineering, Iowa State University, Ames, IA 50011, USA. E-mail: panthani@iastate.edu

[b] Department of Chemistry, Iowa State University, Ames, IA 50011, USA

[c] Ames Laboratory, U.S. Department of Energy, Ames, IA 50011, USA

† Electronic supplementary information (ESI) available: Experimental procedures, and characterization details. Additional XRD patterns, TEM images, XP, FTIR and Raman spectra. Table of Raman peak assignments and vibrational modes for the GeCl$_2$·dioxane complex. See DOI: 10.1039/c9cc01676g
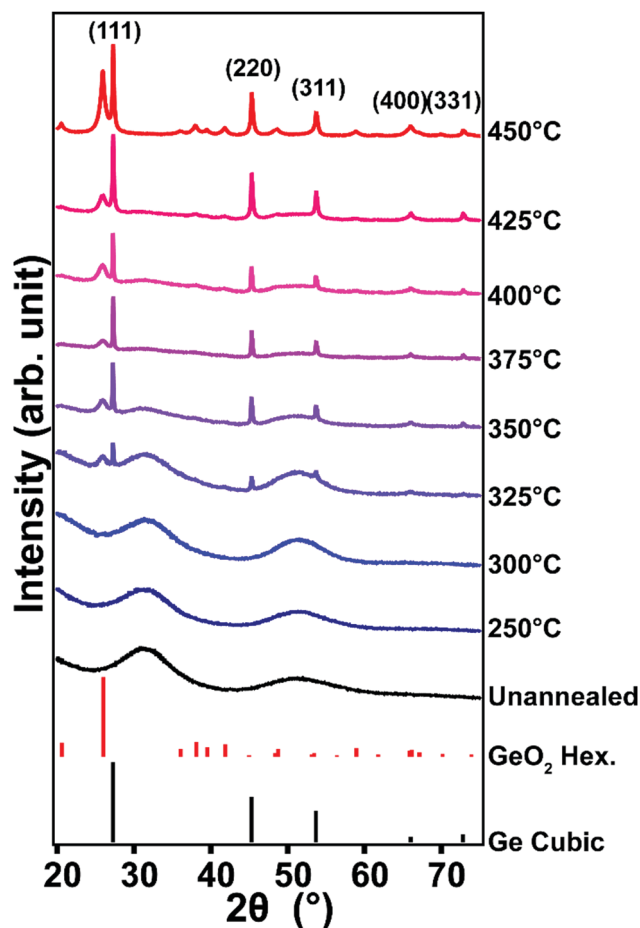
Fig. 1 XRD patterns of hydrolyzed $GeCl_2\cdot$dioxane before and after annealing at various temperatures. Cubic Ge reference: PDF # 00-004-0545, hexagonal GeO_2 reference: PDF # 00-036-1463.

Fig. 2 TEM images of nanocrystals obtained from hydrolyzed $GeCl_2\cdot$dioxane annealed at (a) 375 °C and (b) 425 °C. The insets show the corresponding FFT pattern indexed to diamond cubic Ge.

increase relative to the features corresponding to the amorphous GeO_X. There is relatively little signal indicating the presence of amorphous GeO_X for samples processed at temperatures greater than 400 °C, suggesting that the GeO_X is mostly converted to crystalline Ge and GeO_2. We note the products that are exposed to environments with relatively high humidity (RH $\geq$ 50%) have reflections corresponding to hexagonal GeO_2. However, samples that are prepared in low relative humidity (RH $\leq$ 20%) do not show any reflections corresponding to crystalline GeO_2 (Fig. S2, ESI†), and rather only have broad amorphous features which we assign to amorphous GeO_X, since these features have equivalent width and position to the hydrolyzed $GeCl_2\cdot$dioxane. These data suggest that the formation of crystalline GeO_2 results from exposure to atmospheric moisture. This is in line with a previous experimental study demonstrating that water can cause the transformation of amorphous GeO_2 to hexagonal crystalline GeO_2.[27]

Transmission electron microscopy (TEM) confirms the presence of Ge NCs at annealing temperatures at or above 325 °C (Fig. 2 and Fig. S3, ESI†), with a measured d-spacing of 3.3 Å, consistent with the crystalline cubic Ge(111) plane. Particle size analysis of TEM images suggests that there is no trend in size with respect to
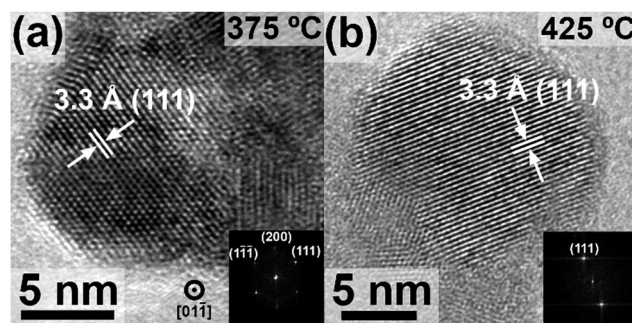
processing temperature. This is different from the observation of Javadi et al. of a clear increase in nanocrystal size with increasing annealing temperature.[25] The Ge NCs are polydisperse and have different morphologies, which could be caused by the two-step heating procedure.[5] The presence of unreacted precursors and amorphous species are also observed in the vicinity of Ge NCs, the presence of which decreases with increasing reaction temperature (Fig. S4–S9, ESI†). This is consistent with XRD data that indicates the decrease of amorphous GeO_X with increasing processing temperature (Fig. 1).

X-ray photoelectron spectroscopy (XPS) measurements quantify the distribution of oxidation states of hydrolyzed $GeCl_2\cdot$dioxane before and after annealing at 250 °C. The measurements suggest a disproportionation process occurs during thermal annealing (Fig. 3 and Fig. S12, ESI†). As shown in Fig. S12 (ESI†), prior to annealing, the hydrolyzed $GeCl_2\cdot$dioxane has signals from Ge, C, O as well as Cl. The presence of Cl likely indicates incomplete conversion of $GeCl_2\cdot$dioxane to $Ge(OH)_2$ during the hydrolysis step. High-resolution XPS (Fig. 3) of the hydrolyzed $GeCl_2\cdot$dioxane before annealing has Ge 3d peak that is dominated by Ge^{2+}, with smaller contributions from Ge^{4+} and Ge^0.[28] The Ge^{2+} signal is attributed to $Ge(OH)_2$ from hydrolysis and unreacted $GeCl_2$, while Ge^{4+} is attributed to surface oxidation. Due to the lack of crystalline features in XRD, the Ge^0 signal likely arises from amorphous Ge from the precursor. After annealing at 250 °C, the peak becomes broader and signals from Ge^0 and Ge^{4+} increases while signal from Ge^{2+} decreases, suggesting that the disproportionation process begins at temperatures as low as 250 °C, supporting the hypothesis that the exotherm in DSC 250 °C is related to the decomposition of the precursor and formation of Ge nuclei.

To better understand the formation of crystalline Ge at unprecedentedly low temperatures, we measured the Raman spectra of the $GeCl_2\cdot$dioxane precursor before and after hydrolysis (Fig. 4a). The peak of $GeCl_2\cdot$dioxane at 316 cm^{-1} is attributed to the Ge phonon mode of a Ge–Cl stretch,[28] and the shoulder around 280 cm^{-1} is attributed to amorphous Ge.[29,30] The entire Raman spectrum of $GeCl_2\cdot$dioxane from 200 to 4000 cm^{-1} is shown in Fig. S13 (ESI†) and detailed Raman peak assignments are shown in Table S1 (ESI†). After hydrolyzing the $GeCl_2\cdot$dioxane, the Ge–Cl stretch becomes relatively weak compared to the amorphous Ge signal, but is still present (Fig. 4a). This is
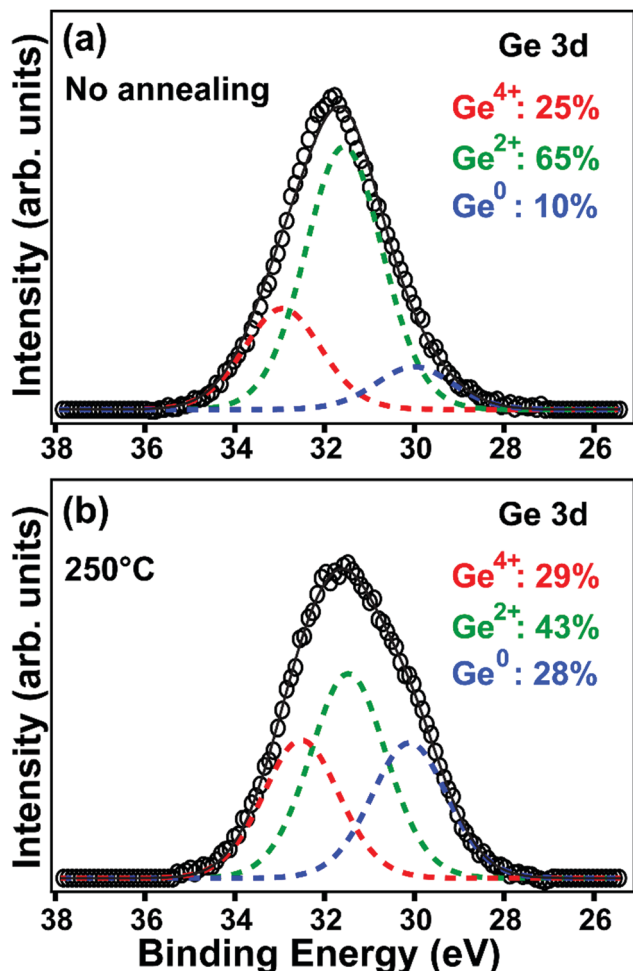
Fig. 3 XPS of hydrolyzed $GeCl_2$·dioxane (a) before annealing, and (b) after annealing at 250 °C. Collected data are shown with open circles. Fitted data are shown in solid curve of black (Ge 3d), dash curves red (Ge^{4+}), green (Ge^{2+}), and blue (Ge^0).

Fig. 4 (a) Baseline-corrected Raman spectra of $GeCl_2$·dioxane precursor before hydrolysis (red) and after hydrolysis (blue). (b) Normalized Raman spectra of hydrolyzed $GeCl_2$·dioxane annealed at temperatures between 250 and 450 °C.

consistent with the Cl signal seen in XPS and confirms the presence of $GeCl_2$ before annealing (Fig. S12, ESI†). Furthermore, a new Raman peak associated with an O–H bond at 3510 cm^{-1} appears after hydrolysis (as shown in Fig. S14, ESI†), indicating that some of the $GeCl_2$ reacted with water to form $Ge(OH)_2$. The presence of the peak associated with amorphous Ge is consistent with the XPS spectra that has photoemission from Ge^0 in the hydrolyzed $GeCl_2$·dioxane (Fig. 3).

After thermally annealing the hydrolyzed precursor at temperatures greater than or equal to 250 °C, peaks corresponding to Ge–Ge begin to appear, with Raman shift of around 285 cm^{-1} (Fig. 4b). This presumably indicates the formation of small Ge NCs or possibly nuclei at temperatures as low as 250 °C, consistent with observation of exotherm in DSC and the Ge^0 from XPS at 250 °C. As shown in Fig. 4b, the Raman peaks become more symmetric, sharper, and shift to higher wavenumbers with increasing processing temperatures (see Fig. S15 for more details, ESI†). Qualitatively, the change in peak shape indicates that the size of the Ge NCs increases with temperature, as is predicted by the phonon confinement model.[30–32]
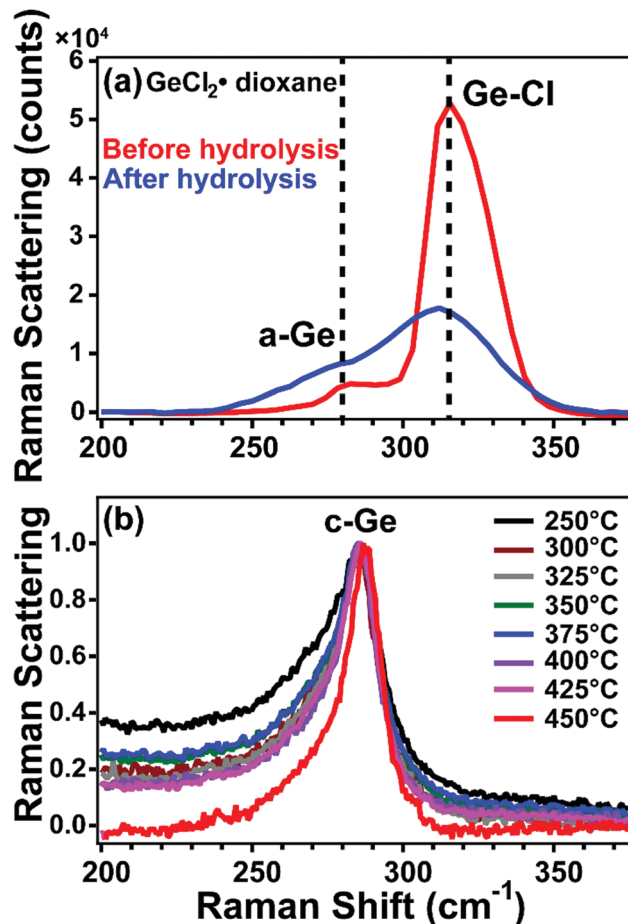
Compared to previous reports of Ge NC synthesis from oxide disproportionation, the approach reported here results in the formation of crystalline Ge at relatively low temperatures.[18,23,24,33] While further work must be done to compare the crystallization dynamics between these approaches, there are some hints as to what could cause the different crystallization temperature. As previously mentioned, the XRD pattern of the hydrolyzed product has different amorphous feature locations from previous reports.[18,23,24,33] Also, Raman and XPS results imply the presence of Ge–Cl bonds (see Fig. S12 (ESI†) for the survey XP spectrum of hydrolyzed $GeCl_2$·dioxane). Ge–Cl bonds have a lower dissociation energy than Ge–O (390.8 ± 9.6 kJ mol^{-1} and 652.7 ± 8.4 kJ mol^{-1}, respectively), suggesting Ge–Cl bonds can dissociate at a lower temperature than Ge–O bonds.[34] We speculate that this could contribute to the formation of Ge NCs at lower temperatures.

The Ge NCs are functionalized using hydrogermylation. Briefly, the annealed GeO_X glass is etched with warm water to dissolve GeO_2 and liberate freestanding Ge NCs, which are then dispersed in HF acid to terminate Ge NCs with hydrogen atoms.[23,24] Finally, the H-terminated Ge NCs are dispersed in 1-octadecene and heated to 200 °C in an inert atmosphere to

initiate hydrogermylation, terminating the Ge NC surfaces with 1-octadecene. TEM images of the passivated sample suggest that the GeO_2 and precursors are removed (Fig. S16, ESI†). The main lattice spacing in selected area electron diffraction (3.3, 2.0, and 1.7 Å) corresponds to crystalline Ge, confirming the presence of Ge NCs. Fourier transform infrared spectroscopy shows the presence of Ge–C stretching mode, indicating the success of surface passivation (Fig. S17, ESI†).

We attempted to measure photoluminescence (PL) from the hydrogen-terminated and 1-octadecene-terminated samples; however, no PL is detected in any sample. The absence of PL could arise from surface defects, dangling bonds from etching, impurities, or surface species that are not adequately removed during the etching process. The absence of PL is also reported for Ge NCs obtained using similar oxide-based solid-state synthesis.[24]

In conclusion, we report the synthesis of Ge NCs using solid-state disproportionation of a chloride-derived GeO_X glass. XRD and TEM results showed the presence of crystalline Ge particles at processing temperature as low as 325 °C. TEM results also indicated the nanocrystals were highly polydisperse with irregular morphologies. XPS and Raman spectra provided insights into the mechanism by which the NCs were formed, with residual Cl present in the GeO_X precursor and Ge with short-range order being formed at temperatures as low as 250 °C. XRD data indicated the GeO_X precursor had amorphous features that were shifted to a higher 2θ compared to prior reports. The Ge NCs obtained with this method could be surface-passivated with an organic ligand using hydrogermylation. Compared to other methods for creating Ge NCs, this method takes relatively little time and does not require the use of strong acids or highly exothermic reactions and thus has potential for being scaled up easily, providing a promising route for large-scale synthesis of Ge NCs for various applications. However, better control over size and morphology would be desirable for many applications.

Conflicts of interest

There are no conflicts to declare.

Notes and references

1 M. L. Steigerwald, A. P. Alivisatos, J. M. Gibson, T. D. Harris, R. Kortan, A. J. Muller, A. M. Thayer, T. M. Duncan, D. C. Douglass and L. E. Brus, *J. Am. Chem. Soc.*, 1988, **110**, 3046–3050.
2 A. Mews, A. V. Kadavanich, U. Banin and A. P. Alivisatos, *Phys. Rev. B: Condens. Matter Mater. Phys.*, 1996, **53**, R13242.
3 A. Cao, Z. Liu, S. Chu, M. Wu, Z. Ye, Z. Cai, Y. Chang, S. Wang, Q. Gong and Y. Liu, *Adv. Mater.*, 2010, **22**, 103–106.
4 C. M. Hessel, D. Reid, M. G. Panthani, M. R. Rasch, B. W. Goodfellow, J. Wei, H. Fujii, V. Akhavan and B. A. Korgel, *Chem. Mater.*, 2012, **24**, 393–401.
5 W. Sun, C. Qian, X. S. Cui, L. Wang, M. Wei, G. Casillas, A. S. Helmy and G. A. Ozin, *Nanoscale*, 2016, **8**, 3678–3684.
6 M. Dasog, G. B. De los Reyes, L. V. Titova, F. A. Hegmann and J. G. C. Veinot, *ACS Nano*, 2014, **8**, 9636–9648.
7 D. C. Lee, J. M. Pietryga, I. Robel, D. J. Werder, R. D. Schaller and V. I. Klimov, *J. Am. Chem. Soc.*, 2009, **131**, 3436–3437.
8 D. A. Ruddy, J. C. Johnson, E. R. Smith and N. R. Neale, *ACS Nano*, 2010, **4**, 7459–7466.
9 M. Kanoun, C. Busseret, A. Poncet, A. Souifi, T. Baron and E. Gautier, *Solid-State Electron.*, 2006, **50**, 1310–1314.
10 Z. C. Holman, C.-Y. Liu and U. R. Kortshagen, *Nano Lett.*, 2010, **10**, 2661–2666.
11 Y. J. Cho, H. S. Im, H. S. Kim, Y. Myung, S. H. Back, Y. R. Lim, C. S. Jung, D. M. Jang, J. Park, E. H. Cha, W. I. Cho, F. Shojaei and H. S. Kang, *ACS Nano*, 2013, **7**, 9075–9084.
12 X. Ma, B. Yuan and Z. Yan, *Opt. Commun.*, 2006, **260**, 337–339.
13 B. R. Taylor, S. M. Kauzlarich, H. W. H. Lee and G. R. Delgado, *Chem. Mater.*, 1998, **10**, 22–24.
14 X. Ma, F. Wu and S. M. Kauzlarich, *J. Solid State Chem.*, 2008, **181**, 1628–1633.
15 R. Gresback, Z. Holman and U. Kortshagen, *Appl. Phys. Lett.*, 2007, **91**, 093119.
16 E. J. Henderson, M. Seino, D. P. Puzzo and G. A. Ozin, *ACS Nano*, 2010, **4**, 7683–7691.
17 M. Hoffman and J. G. C. Veinot, *Chem. Mater.*, 2012, **24**, 1283–1291.
18 E. J. Henderson, C. M. Hessel and J. G. C. Veinot, *J. Am. Chem. Soc.*, 2008, **130**, 3624–3632.
19 X. Lu, K. J. Ziegler, A. Ghezelbash, K. P. Johnston and B. A. Korgel, *Nano Lett.*, 2004, **4**, 969–974.
20 A. Bernard, K. Zhang, D. Larson, K. Tabatabaei and S. M. Kauzlarich, *Inorg. Chem.*, 2018, **57**, 5299–5306.
21 E. Muthuswamy, A. S. Iskandar, M. M. Amador and S. M. Kauzlarich, *Chem. Mater.*, 2013, **25**, 1416–1422.
22 X. Lu, B. A. Korgel and K. P. Johnston, *Chem. Mater.*, 2005, **17**, 6479–6485.
23 W. Sun, G. Zhong, C. Kübel, A. A. Jelle, C. Qian, L. Wang, M. Ebrahimi, L. M. Reyes, A. S. Helmy and G. A. Ozin, *Angew. Chem.*, 2017, **129**, 6426–6431.
24 M. Javadi, D. Picard, R. Sinelnikov, M. A. Narreto, F. A. Hegmann and J. G. C. Veinot, *Langmuir*, 2017, **33**, 8757–8765.
25 M. Javadi, V. K. Michaelis and J. G. C. Veinot, *J. Phys. Chem. C*, 2018, **122**, 17518–17525.
26 N. N. Greenwood and A. Earnshaw, *Chemistry of the Elements*, Elsevier, 2012.
27 Z. Xiao, Z. Sun, X. Li, Y. Wang, Z. Wang, B. Zhang, X. L. Li, Z. Shen, L. B. Kong and Y. Huang, *Nano Lett.*, 2018, **18**, 3290–3296.
28 G. A. Ozin and A. V. Voet, *J. Chem. Phys.*, 1972, **56**, 4768–4775.
29 D. Bermejo and M. Cardona, *J. Non-Cryst. Solids*, 1979, **32**, 405–419.
30 M. Fujii, S. Hayashi and K. Yamamoto, *Jpn. J. Appl. Phys.*, 1991, **30**, 687.
31 I. H. Campbell and P. M. Fauchet, *Solid State Commun.*, 1986, **58**, 739–741.
32 A. K. Arora, M. Rajalakshmi, T. R. Ravindran and V. Sivasubramanian, *J. Raman Spectrosc.*, 2007, **38**, 604–617.
33 A. Schacht, C. Sternemann, A. Hohl, H. Sternemann, C. J. Sahle, M. Paulus and M. Tolan, *J. Non-Cryst. Solids*, 2009, **355**, 1285–1287.
34 Y.-R. Luo, *Comprehensive Handbook of Chemical Bond Energies*, CRC Press, 2007.